The Human Brain Connectome Weighted by the Myelin Content and Total Intra-Axonal Cross-Sectional Area of White Matter Tracts

Short title:

Mark C. Nelson[1,2], Jessica Royer[1,2], Ilana R. Leppert[2], Jennifer S.W. Campbell[2], Simona Schiavi[3], Hyerang Jin[1,2], Shahin Tavakol[1,2], Reinder Vos de Wael[1,2], Raul Rodriguez-Cruces[1,2], G. Bruce Pike[4], Boris C. Bernhardt[1,2], Alessandro Daducci[3], Bratislav Misic[1,2], and Christine L. Tardif [1,2,5]

[1]*Department of Neurology and Neurosurgery, McGill university, Montreal, QC, Canada.* [2]*McConnell Brain Imaging Centre, Montreal Neurological Institute and Hospital, Montreal, QC, Canada.* [3]*Department of Computer Science, University of Verona, Verona, Italy.* [4]*Hotchkiss Brain Institute and Departments of Radiology and Clinical Neuroscience, University of Calgary, Calgary, Canada.* [5]*Department of Biomedical Engineering, McGill University, Montreal, QC, Canada.*

Corresponding Author: Mark C Nelson, mark.nelson3@mail.mcgill.ca

Keywords: connectomics; network neuroscience; structural connectivity; functional connectivity; white matter; myelin; computational modeling

ABSTRACT

A central goal in neuroscience is the development of a comprehensive mapping between structural and functional brain features. Computational models support *in vivo* investigation of the mechanisms mediating this relationship but currently lack the requisite biological detail. Here, we characterize human structural brain networks weighted by multiple white matter

microstructural features to assess their potential joint utilization in computational models. We report edge-weight-dependent spatial distributions, variance, small-worldness, rich club, hubs, as well as relationships with function, edge length and myelin. Contrasting networks weighted by the total intra-axonal cross-sectional area and myelin content of white matter tracts, we find opposite relationships with functional connectivity, an edge-length-independent inverse relationship with each other, and the lack of a canonical rich club in myelin-weighted networks. When controlling for edge length, tractometry-derived networks weighted by either tensor-based metrics or neurite density show no relationship with whole-brain functional connectivity. We conclude that structure-function brain models are likely to be improved by the co-utilization of structural networks weighted by total intra-axonal cross-sectional area and myelin content. We anticipate that the proposed microstructure-weighted computational modeling approach will support mechanistic understanding of the structure-function relationship of the human brain.

AUTHOR SUMMARY

For computational network models to provide mechanistic links between brain structure and function, they must be informed by networks in which edge weights quantify structural features relevant to brain function. Here, we characterized several weighted structural networks capturing multiscale features of white matter connectivity. We describe these networks in terms of edge weight distribution, variance and network topology, as well as their relationships with each other, edge length and function. Overall, these findings support the joint use of structural networks weighted by the total intra-axonal cross-sectional area and myelin content of white matter tracts

in structure-function models. This thorough characterization serves as a benchmark for future investigations of weighted structural brain networks.

INTRODUCTION

The quest to relate human structural and functional brain networks spans the spectrum of spatial scale and repertoire of data modalities absolutely. At the macroscale, the human brain can be modeled as an anatomical network of discrete neuronal populations (nodes) interconnected by white matter fibers (edges) (Sporns, 2011). Coordinated spatiotemporal patterns of neuronal activity unfolding upon this structural backbone are fine-tuned by white matter microstructure (Hodgkin & Huxley, 1952; Huxley & Stämpfli, 1949; Moore et al., 2020; Pumphrey & Young, 1938) and form the basis of cognition and behavior (Biswal et al., 1995; Greicius et al., 2003; Hampson et al., 2006; Liégeois et al., 2019; S. M. Smith et al., 2009; Martijn P. Van Den Heuvel et al., 2009). Increasingly, MRI facilitates *in vivo* measurement of multi-scale properties of both brain structure (e.g., (Alexander et al., 2019; Drakesmith et al., 2019; Jeurissen et al., 2017; Mancini et al., 2020)) and function (e.g., (Finn et al., 2019; Friston, 2011; Gordon et al., 2017; Liu et al., 2022)). Diffusion MRI streamline tractography and resting-state functional MRI are often respectively used to estimate structural and functional connectivity (SC & FC) networks. Network science provides a framework to bring these fundamentally different substrates into a common space where their features can be quantified (Fornito et al., 2016; Sporns, 2010; Suárez et al., 2020) and used to probe the mechanisms mediating human brain function (e.g., (Cabral et al., 2017; Fornito et al., 2015)).

SC network edges can be weighted by a range of MRI-derived metrics quantifying white matter microstructural features relevant to brain function including voxel-level estimates of tissue diffusivity (e.g., (Caeyenberghs et al., 2016)), neurite density (Zhang et al., 2012), axon diameter distributions (Alexander et al., 2010; Assaf et al., 2008), myelin content (Heath et al., 2018; Mancini et al., 2020), and the g-ratio (ratio of inner/outer diameters of myelinated axons) (Stikov et al., 2011, 2015); as well as tract/bundle-level measures of axonal cross-sectional area (Daducci, Dal Palù, et al., 2015; R. E. Smith et al., 2015). Subsets of these metrics have been investigated using a microstructure-weighted connectomics approach (Boshkovski et al., 2021; Caeyenberghs et al., 2016; Deligianni et al., 2016; Frigo et al., 2020; Mancini et al., 2018; Messaritaki et al., 2021; Schiavi et al., 2020; M. P. van den Heuvel et al., 2010; Martijn P. van den Heuvel & Sporns, 2011; F. C. Yeh et al., 2016), however a comprehensive characterization has not yet been provided.

Our goal is to characterize a range of standard and state-of-the-art weighted structural brain networks in support of their utilization in computational models of brain function. The networks considered here can be grouped into two classes: those computed with tractometry (S Bells et al., 2011) and those computed directly from the streamline weights in a tractogram i.e., streamline-specific. We consider three examples of the latter: (1) the number of streamlines (NoS); and two methods which optimize the streamline weights in a tractogram to increase specificity for white matter structural features (2) spherical-deconvolution informed filtering of tractograms (SIFT2) (R. E. Smith et al., 2015) and (3) convex optimization modeling for microstructure informed tractography (COMMIT) (Daducci et al., 2013; Daducci, Dal Palù, et al., 2015). SIFT2 and

COMMIT were designed to overcome known limitations of streamline counts (Girard et al., 2014; Jones, 2010; Jones et al., 2013). While the edge weights in all three networks generally capture white matter features relevant to connection strength, SIFT2 and COMMIT more specifically quantify the total intra-axonal cross-sectional area of white matter tracts (henceforth referred to as "edge caliber"). To date, SIFT2 and COMMIT have not been compared to NoS with uniform connection density (Frigo et al., 2020; Schiavi et al., 2020; C. H. Yeh et al., 2016). Thus, it remains unclear how the edge weights themselves affect network topology.

In contrast, tractometry allows network edge weights to be derived from any volumetric brain image that is co-registered to the tractogram. This increase in methodological flexibility comes at the expense of anatomical specificity. Tractometry is unable to resolve the separate contributions of individual fiber populations to the aggregate value of a voxel. Given that an estimated ~90% of white matter voxels at typical diffusion MRI resolutions (~2mm) contain multiple fiber populations (Jeurissen et al., 2012), the quantitative link between white matter microstructure and essentially all tractometry-derived edge weights is biased by partial volume effects.

In this work, tractometry is combined with a diffusion tensor model (Basser, 1995; Basser et al., 1994) to derive networks weighted by FA (fractional anisotropy) and RD (radial diffusivity), which respectively quantify the degree of diffusion anisotropy (i.e., directional dependence) and diffusion magnitude perpendicular to the major axis. The crossing fiber problem described above is also known to limit the ability of diffusion tensor models to quantify white matter features (De Santis et al., 2014; J. D. Tournier et al., 2011). Additional tractometry networks examined here include a network weighted by ICVF (intracellular volume fraction) computed with NODDI

(Neurite Orientation Dispersion and Density Imaging) (Zhang et al., 2012), as well as a network weighted by the longitudinal relaxation rate R_1 ($1/T_1$), which has been shown to correlate with histology-derived myelin content (Mottershead et al., 2003).

This characterization of weighted structural brain networks is carried out as follows: (1) within-network features of edge weight distribution and variance; (2) edgewise relationships with FC, edge length and myelin (R_1); and (3) topological features of small-worldness, rich club and network hubs. Importantly, uniform binary connectivity is enforced across all weighted network variants allowing the edge weights themselves to drive the characterization.

RESULTS

In 50 healthy adults (27 men; 29.54±5.62 years; 47 right-handed), structural brain networks were estimated from multi-shell diffusion MRI data with probabilistic tractography. Each subject's structural network was used to compute 8 SC networks in which edges were weighted by: NoS, SIFT2, COMMIT, FA, RD, ICVF, R_1 and LoS (edge length computed as the mean length of streamlines). The edge weights in NoS, SIFT2 and COMMIT networks were normalized by node volume. Additionally, a static FC network was derived for each subject by zero-lag Pearson cross-correlation of nodewise resting-state time series. Unless otherwise stated, all results shown correspond to networks parcellated with the Schaefer-400 cortical atlas (Schaefer et al., 2018) and include 14 subcortical nodes.

Structural Brain Networks Vary in the Distribution of Their Edge Weights

Group-level networks weighted by NoS, SIFT2 and COMMIT show spatially distributed patterns of high magnitude edge weights and noticeably accentuate within-module connectivity (**Figure 1A**). Modules correspond to the 7-canonical resting-state networks (Thomas Yeo et al., 2011) plus the subcortex. These patterns are hallmarks of FC networks and are observed in the FC network shown here. The contrast between high and low magnitude edge weights is most evident in COMMIT. By comparison, the spatial variation of edge weight distribution in the tractometry networks is smoother with more pronounced regional concentrations. R_1 is highest in the edges connecting the visual module to itself and to the rest of the brain; and lowest within the subcortex and between the subcortical and limbic modules. The surface plot shows the highest concentration of R_1 in the white matter projections of posterior cortical regions.

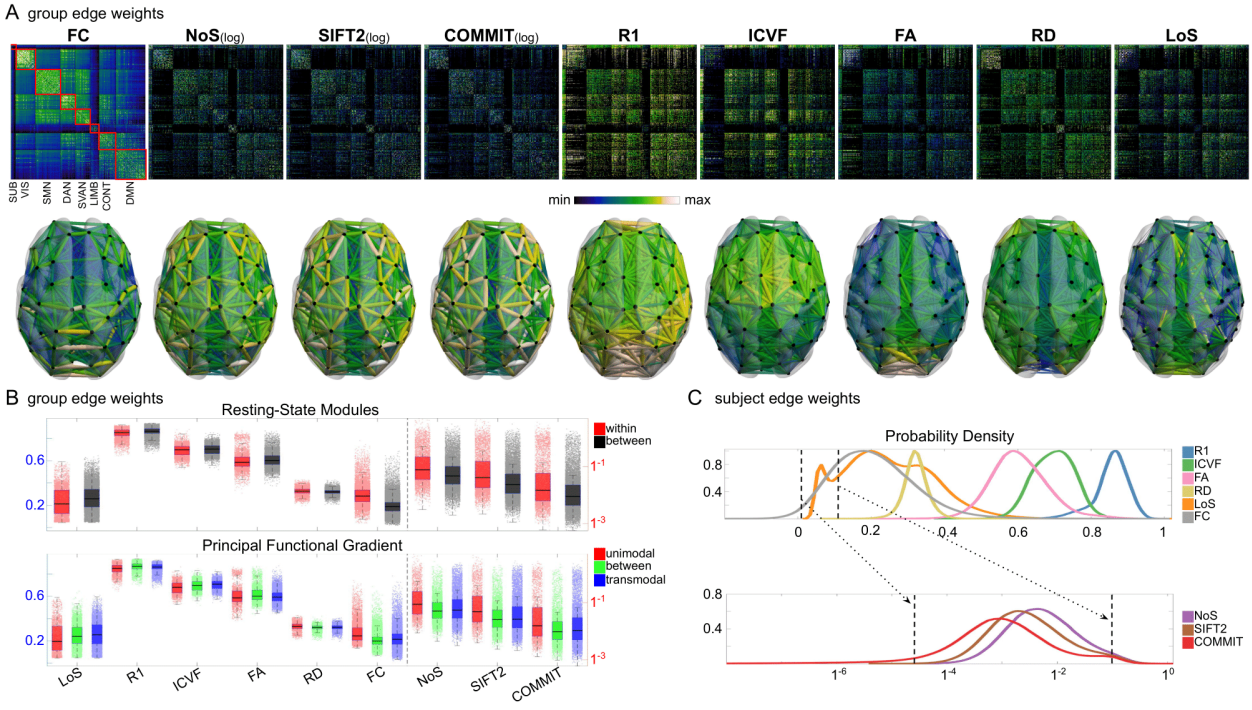

***Figure 1**. Edge Weight Distribution. (A) Connectivity matrices (top row) of group-level edge weights for FC (functional connectivity), NoS (number of streamlines), SIFT2 (spherical-deconvolution informed filtering of tractograms), COMMIT (convex optimization modeling for microstructure informed tractography), R_1 (longitudinal relaxation rate), ICVF (intra-cellular*

volume fraction), FA (fractional anisotropy), RD (radial diffusivity) and LoS (mean length of streamlines). Each network is composed of 414 nodes as defined by the Schaefer-400 cortical parcellation and 14 subcortical ROIs. Nodes are grouped into the canonical resting state modules (Thomas Yeo et al., 2011) *plus the subcortex: SUB (subcortex), VIS (visual), SMN (somatomotor), DAN (dorsal attention), SVAN (salience ventral attention), LIMB (limbic), CONT (control), and DMN (default mode). 3D cortical surfaces (bottom row) of group-level edge weights in the Schaefer-100 parcellation generated with BrainNet Viewer* (Xia et al., 2013)*. Edge diameter and color indicate weight magnitude. (B) Distribution of group-level edge weights binned by: (top) within and between module; (bottom) unimodal, transmodal and between. Unimodal is defined as the VIS and SMN modules. Transmodal is defined as the DMN, CONT, DAN and SVAN modules. (C) Probability density of pooled subject-level edge weight distributions. R_1, ICVF, FA, RD, LoS and FC are shown on a linear x-axis (top), and NoS, SIFT2 and COMMIT are shown on a logarithmic x-axis (bottom). All networks were normalized to the range [0 1] by dividing by the subject-level max for visualization. The edge weights in NoS, SIFT2 and COMMIT networks were log_{10} transformed for these plots.*

Group-level edge weight distributions are summarized with respect to two important organizational patterns of brain function (**Figure 1B**): within and between resting state modules (Thomas Yeo et al., 2011); and along the principal functional gradient (Margulies et al., 2016). NoS, SIFT2 and COMMIT mirror FC in both plots with greater edge weight magnitude within module, especially within unimodal modules. R_1, ICVF, FA and RD generally mirror LoS with the reverse trend: higher between module and lowest in unimodal modules. This suggests that tractometry-derived networks may be influenced by edge length to a greater extent.

Subject-level edge weight distributions in R_1, ICVF, FA and RD are near-normal and network-specific (**Figure 1C**). They differ in both the magnitude (R_1 > ICVF > FA > RD) and dynamic range (FA & ICVF > R_1 & RD) of their edge weights. In contrast, NoS, SIFT2 and COMMIT distributions are highly skewed and tend to be much lower in magnitude (dashed lines). This effect is greatest in COMMIT suggesting that the optimization performed by COMMIT exerts a stronger scaling effect than SIFT2. These results support the conclusion that the structural networks considered here quantify subsets of white matter features which are at least partially non-overlapping.

184 ***Edge Weights in Streamline-Specific Networks Are More Variable***

185 Edge weight variance was quantified using the Quartile Coefficient of Dispersion (CQD) due to
186 its robustness to outliers and skewed data. The CQD is computed from the 1st and 3rd quartiles as:
187 $CQD = Q_3 - Q_1 \,/\, Q_3 + Q_1$.
188
189 *Intra-subject* variance is roughly 2-fold greater in NoS, SIFT2 and COMMIT than LoS and FC;
190 and an order of magnitude greater than R_1, ICVF, FA and RD in all subjects (**Figure 2A**).
191 COMMIT is the highest overall. Subjects are more tightly clustered in all weighted SC networks,
192 relative to FC: *intra-subject* CQD values span roughly a 4-fold greater range in FC. This
193 suggests that individual diversity of functional connectivity is not necessarily reflected in the
194 variability of their structural networks. These patterns are repeated for *inter-subject* variance.
195 However, FC shows a small subset of highly variable edges with roughly 4-fold greater CQD
196 than the maximum values observed in COMMIT i.e., the most subject-specific connections are
197 functional. The very low edge weight variability in R1, ICVF, FA and RD is in part due to the
198 widespread smoothing effect (partial voluming) resulting from the tractometry computation.
199

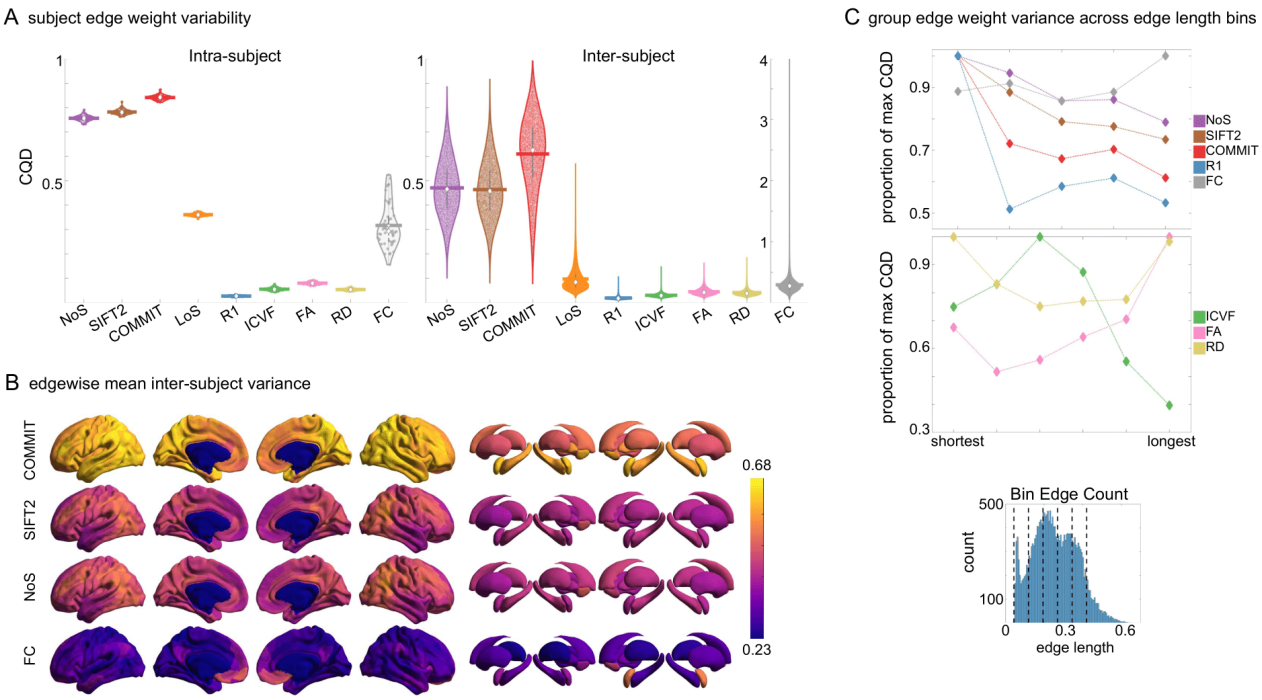

***Figure 2**. Edge Weight Variability. Variability is quantified using the coefficient of quartile dispersion (CQD). (A) Violin distributions of **intra-subject** (left) and **inter-subject** (right) edge weight variance. Colored data points respectively correspond to individual subjects (N=50) and edges (N=8549). (B) Surface projections of edgewise mean inter-subject variance for cortical nodes in the Schaefer-400 parcellation (left) and 14 subcortical nodes (right). Cortical and subcortical surfaces were respectively generated with BrainSpace* (Vos de Wael et al., 2020) *and ENIGMA toolboxes* (Larivière et al., 2021). *(C) The proportion of within-network max CQD is shown across edge length bins for FC, NoS, SIFT2, COMMIT and R_1 (top), as well as ICVF, FA and RD (middle). Edge weights are grouped into 6 bins according to edge length, as illustrated by the histogram (bottom). The edges of bins 1-5 were linearly spaced of width, w. The edges of the final bin were of width 3w.*

In general, *inter-subject* edge weight variance is more spatially distributed in SC networks relative to FC (**Figure 2B**). COMMIT shows the highest mean CQD over the entire cortex and subcortex. NoS, SIFT2 and COMMIT all show lateral-medial and posterior-anterior cortical gradients. Mean CQD in FC shows the highest concentration in medial inferior frontal cortex and to a lesser extent, the expected pattern of high variance in association cortex. The most variable subcortical regions include the hippocampus, amygdala and accumbens.

Many features of brain networks (e.g., connection probability, weight magnitude) are known to vary with edge length. Here, we examined the relationship between edge weight variability and

edge length by computing the CQD within subsets of group-level edge weights binned according to their edge length (**Figure 2C**). Edge weight variance in NoS, SIFT2, COMMIT and R_1 is highest in the shortest edges and decreases with edge length. ICVF roughly follows the same pattern. FA and RD instead show the highest variability in the longest edges. Overall, the edge weights in streamline-specific SC networks (NoS, SIFT2 and COMMIT) show greater contrast both within and across subjects. SC networks show network-dependent relationships between edge weight variance and edge length. Shorter edges are more variable in myelin- and connection strength-weighted networks, and longer edges are more variable in networks with edge weights derived from a diffusion tensor model.

Opposing Correlations with Function in Connection-Strength- & Myelin-Weighted Networks

Shifting to inter-network edge weight relationships shows that SC networks are differentially related to FC (**Figure 3A)**. Importantly, we also see that all brain networks (SC and FC) are strongly and differentially related to edge length at the subject and group levels. Correlations with edge length are negative for NoS, SIFT2, COMMIT, RD and FC; and positive for R_1, ICVF, and FA. Correlation magnitude is strongest in group-level COMMIT ($\rho \approx -0.8$). To remove this strong obscuring effect, we recomputed correlations using residual edge weights following linear regression of edge length (**Figure 3B**). NoS, SIFT2 and COMMIT remain positively associated (group-level $\rho \approx 0.35$) and R_1 remains negatively associated with FC (group-level $\rho \approx -0.22$). Correlation magnitude was reduced following linear regression in all cases. ICVF, FA and RD are reduced to 0 suggesting that they may not be useful in modeling whole-brain FC. These results support the idea that R_1-weighted SC networks provide

242 complementary information to NoS, SIFT2 and COMMIT about the brain structure-function
243 relationship.
244

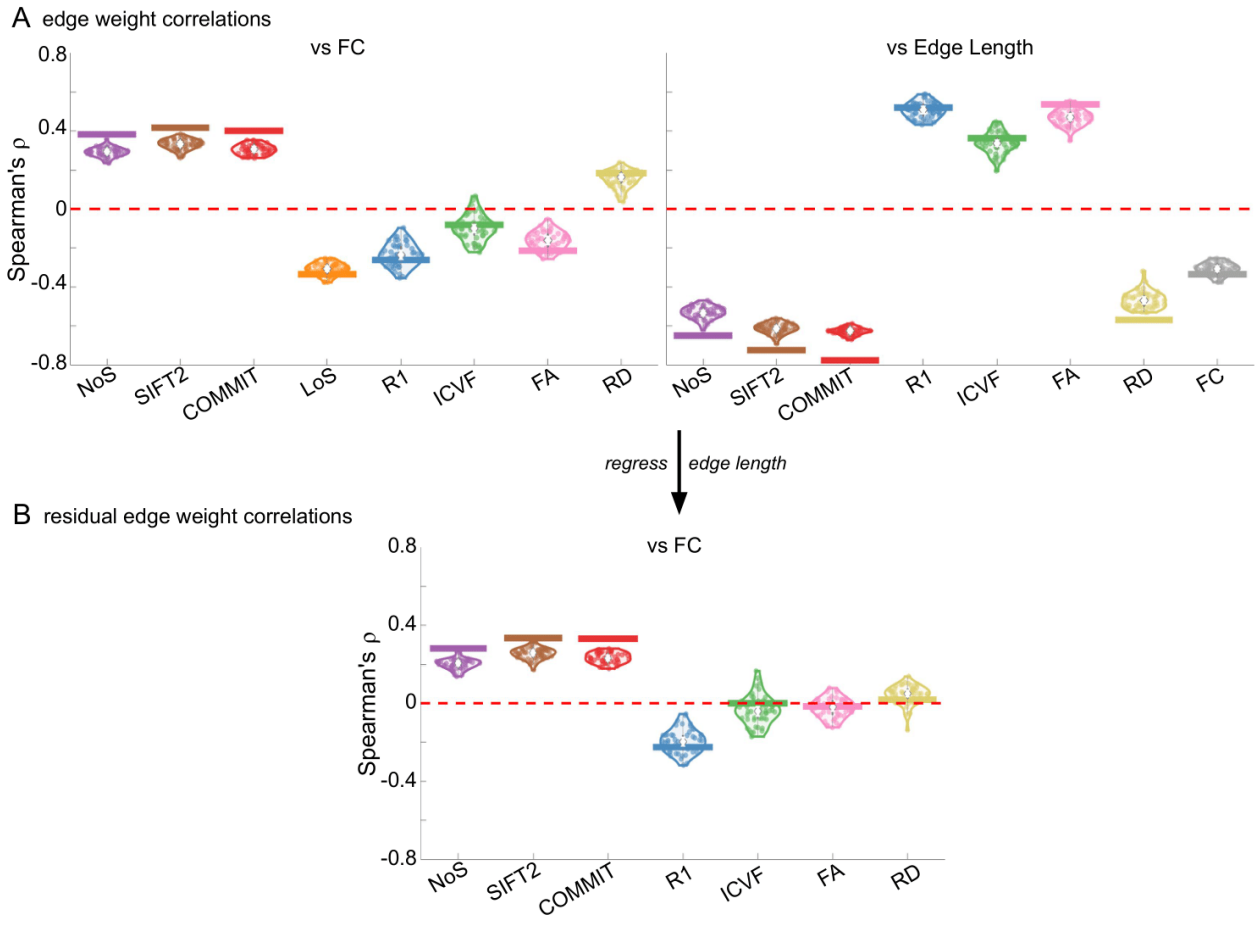

245

246 ***Figure 3***. *Edge Weight Correlations with FC and Edge Length. (A) Violin distributions of edgewise Spearman's rank*
247 *correlations of all networks with FC (left) and edge length (right). (B) Violin distributions of edgewise Spearman's rank*
248 *correlations of residual edge weights in all networks with residual edge weights in FC. Residual edge weights were computed by*
249 *linear regression of edge length. Colored data points and bars respectively indicate subject-level and group-level correlations.*

250

251

252 ***Edge Caliber and Myelin Content are Inversely Related***

253 Here, we ask how R_1, which we refer to as the myelin-weighted network, is related to the
254 connection-strength-weighted network COMMIT. Edge-length regressed residual edge weights
255 in NoS, SIFT2 and COMMIT show a negative association with R_1 residuals for all subjects and

256 at the group level, which is strongest in COMMIT (group-level ρ & r ≈ -0.29) (**Figure 4A**). This
257 suggests an edge-length independent inverse relationship between white matter structural
258 features related to connection strength and myelin content.
259

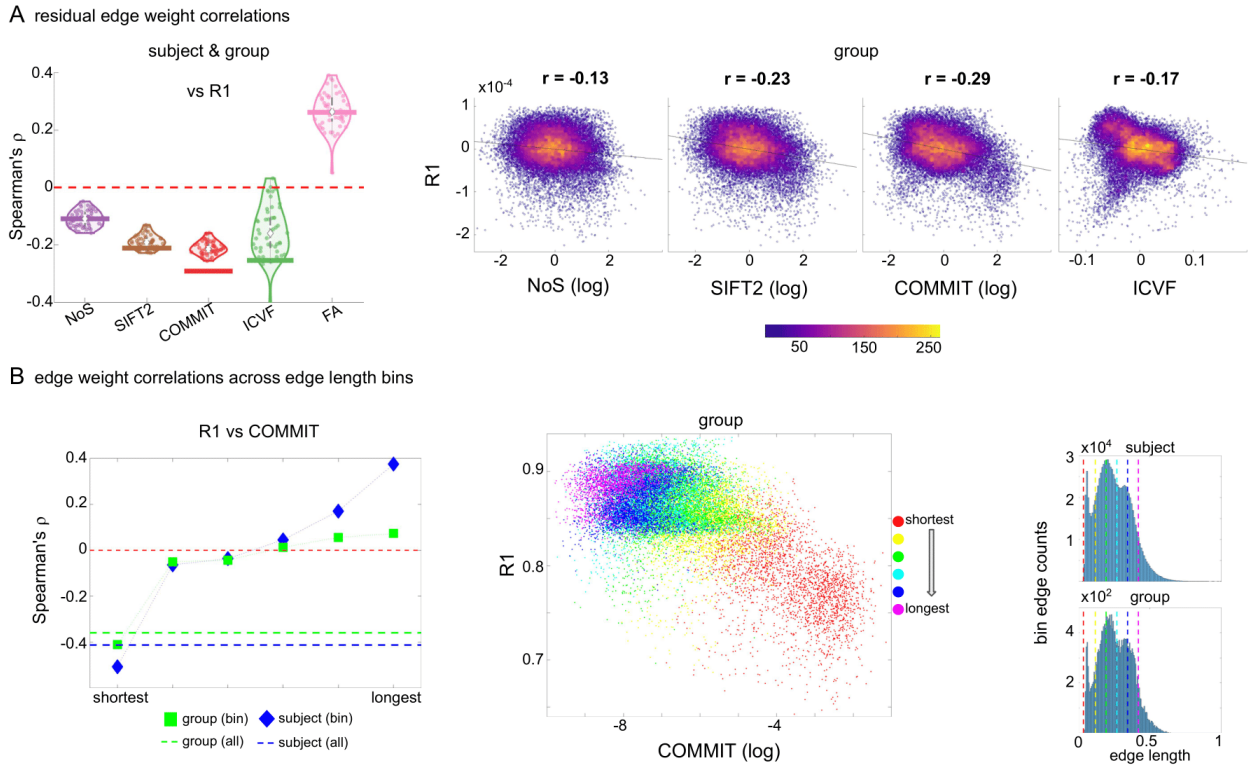

260

261 ***Figure 4****. The Myelin-Dependence of Structural Brain Networks. (A) Violin distributions (left) of edgewise Spearman's rank*
262 *correlations with the myelin-weighted network R_1. Residual edge weights are compared following linear regression of edge*
263 *length. Colored data points and bars respectively indicate subject-level and group-level correlations. Heat scatter plots (right) of*
264 *group-level residual edge weights in R_1 as a function of NoS (left), SIFT2 (left middle), COMMIT (right middle) and ICVF (right)*
265 *with the best fit linear curve shown in black. Color indicates data density. (B) Line plot (left) of edgewise Spearman's rank*
266 *correlation of edge weights in R_1 vs COMMIT across edge length bins. Group-level and subject-level are respectively shown in*
267 *green and blue. The square and diamond markers connected by dotted lines show binned correlation values, and the horizontal*
268 *dashed green and blue lines mark the correlation values for all edges pooled together. Scatter plot (middle) of group-level edge*
269 *weights in R_1 as a function of COMMIT with data points colored by bin identity. Histograms (right) illustrating subject- and*
270 *group-level edge length bins.*

271

272 Computing correlations of edge weights (not residuals) within edge-length bins allows the
273 inverse relationship between R_1 and COMMIT to be traced to the shortest edges of the network
274 (group ρ ≈ -0.40, subject ρ ≈ -0.50). As edge length increases, this relationship is reduced to 0,

then becomes strongly positive in the longest subject-level edges ($\rho \approx 0.39$). The scatter plot of group-level R_1 vs COMMIT (middle) shows decreasing COMMIT and increasing R_1 with increasing edge length. All together, these results support an inverse relationship between the edge caliber and myelin content of a given white matter tract. This can be partly explained by the differential dependence of these structural features on edge length: longer tracts tend to be more myelinated with lower total intra-axonal cross-sectional area. However, this relationship is robust to controlling for edge length supporting an intrinsic dependence between these white matter features.

Divergent Small-Worldness, Hubness and Rich Club in Weighted Structural Networks

In this final section, we apply network analysis tools (Rubinov & Sporns, 2010) based on graph theory (Fornito et al., 2013; Sporns, 2018) to group-level weighted SC networks. This facilitates high-level interpretation of general features of network communication such as integrative vs segregative processing and the economy of network organization. Although the high material and metabolic cost of brain tissue naturally tends to favor local connectivity (high clustering), short overall network path length is achieved through a small number of relatively expensive long-range connections (Bullmore & Sporns, 2012). These edges and the nodes they interlink form a densely connected network core known as the rich club (Martijn P. van den Heuvel & Sporns, 2011). While the general proclivity for high local clustering gives rise to segregated functional modules, the rich-club nodes act as network communication hubs supporting inter-modular integration (Collin et al., 2014; de Reus & van den Heuvel, 2014; Griffa & Van den Heuvel, 2018; Kim & Min, 2020; Martijn P. van den Heuvel & Sporns, 2013). Thus, small-world network topology (high clustering and low path length) (Bassett & Bullmore, 2006, 2017)

supports both integrative and segregative processing at a minimum of wiring cost, and the underlying scaffold of hub brain regions tend to show high centrality, low path length (high closeness) and low clustering (M. P. van den Heuvel et al., 2010).

Here, we report normalized small-worldness, normalized rich-club curves and nodal hubness (**Figure 5**). Normalized small-worldness (S) is computed as the quotient of normalized measures of clustering coefficient (C/C_{null}) and path length (L/L_{null}).

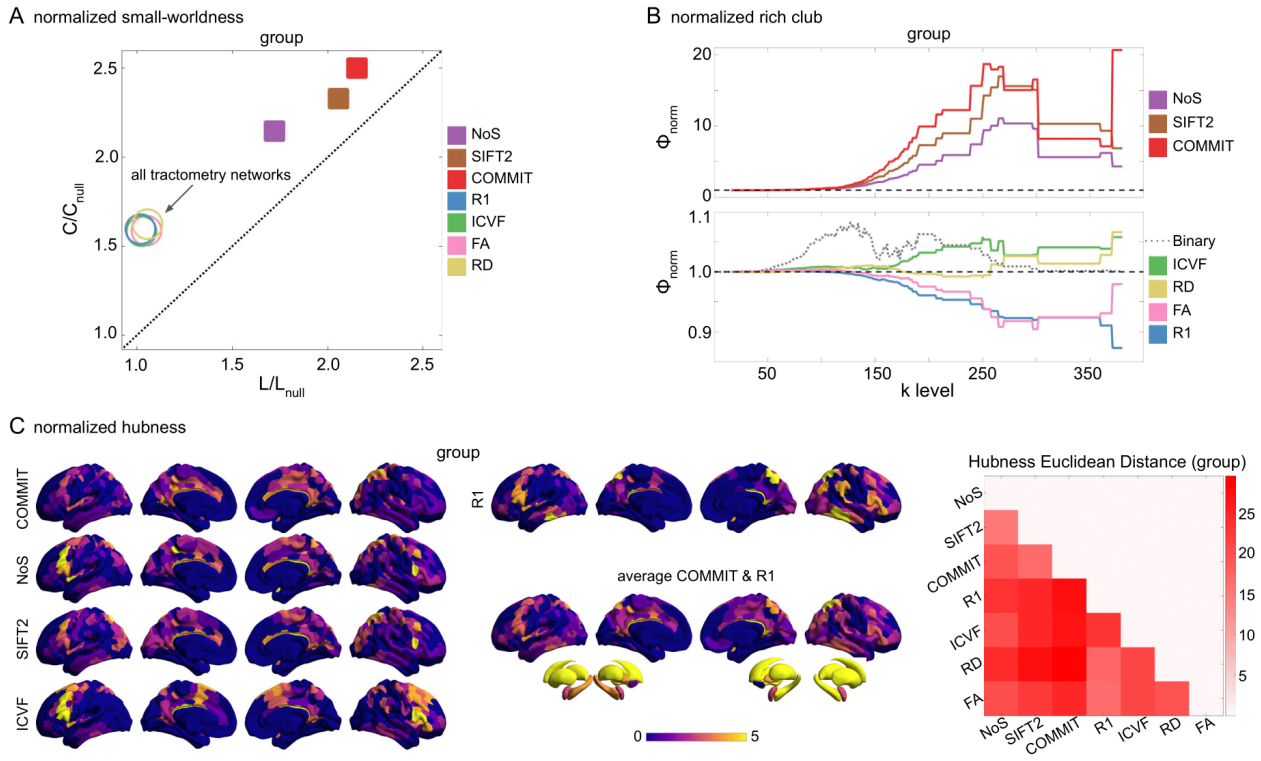

***Figure 5**. Group-level network topology. (A) Small-worldness was estimated in all structural networks: clustering coefficient was normalized within each node, averaged across nodes (C/C_{null}), then plot as a function of normalized Characteristic path length (L/L_{null}). Topology measures averaged across 50 degree and strength preserving null networks were used for normalization. Networks above the identity line (dotted black) are characterized by the small world attribute. Tractometry networks are indicated by the arrow. (B) Normalized rich club curves are shown for COMMIT, NoS and SIFT2 (top), as well as ICVF, RD, FA and R_1 (bottom). A single binary network (dotted gray line) is also shown (bottom) as binary connectivity was uniform across weighted networks. The normalized rich club coefficient (ϕ_{norm}) was computed across the range of degree (k) and normalized against 1000 null models (degree preserving for binary and degree and strength preserving for weighted networks). A ϕ_{norm} value > 1 (horizontal dashed black lines) over a range of k indicates the presence of a rich club. (C) Nodewise hubness scores are projected onto Schaefer-400 cortical and 14-ROI subcortical surfaces. Scores (0-5) were computed for each node as +1 point for*

all nodes in top 20% strength, betweenness, closeness and eigenvector centrality, as well as bottom 20% clustering coefficient. The matrix (right) shows the Euclidean distance between all pairs of nodal hubness vectors.

All group-level weighted SC networks show the normalized small-world property ($S > 1$) of higher clustering and lower path length than would be expected by chance (**Figure 5A**). Small-worldness is highest in COMMIT ($S \approx 2.5$) and lowest in R_1, ICVF, FA and RD ($S \approx 1.6$). In contrast, all weighted SC networks did not show a canonical rich club (**Figure 5B**). Relative to the tractometry and binary SC networks, the normalized rich-club coefficient (ϕ_{norm}) was much higher in magnitude in NoS, SIFT2 and COMMIT. A rich club was detected in these networks across a large range of degree (k) levels ($150 < k < 300$). ϕ_{norm} was maximal at $k \approx 265$ in COMMIT. A rich club was also detected across a similar range of k levels in ICVF and across k in the range [250 300] for RD, albeit with much lower magnitude ϕ_{norm}. However, no clear rich club was observed in R_1 or FA. In fact, the rich-club curves for these networks are roughly symmetric about the $\phi_{norm} = 1$ line relative to COMMIT. A densely connected core was of course recovered in all weighted SC networks (uniform binary connectivity), but these results suggest that its interconnecting edges were consistently weaker than would be expected by chance in R_1 and FA. By comparison, a rich club was observed in the binary SC network across the very large range of k [50 300]. This supports two important concepts: (1) SC network edge weights can provide an additional layer of information useful for refining the topology of binary SC; and (2) different methods for computing SC network edge weights yield diverse network topology.

Weighted SC networks show network-dependent spatial topology of hubness scores (**Figure 5C**). The COMMIT and R1 averaged surface shows prominent hubs distributed throughout the brain including the fronto-parietal network. Nearly all of the subcortex showed a hubness score

of 4 or greater in all networks. The Euclidean distance between hubness score vectors (right) was lower for COMMIT and SIFT2 than for either network with NoS. Of the streamline-specific networks, NoS was more similar to both R1 and IVCF. Overall, these results illustrate the considerable impact that edge weighting can have on network topology.

DISCUSSION

Computational network modeling provides a customizable platform for probing the mechanistic relationship between human brain structure and function *in vivo*. Here, we assemble a thorough characterization of structural brain networks weighted by a range of quantitative MRI metrics capturing the macro- and microscopic features of white matter tracts to inform their utilization in computational models of brain function. Notable trends included: (1) greater edge weight contrast and skewed (heavy-tailed) distributions in the streamline-specific networks NoS, SIFT2 and COMMIT; (2) whole-brain correlations with FC in networks weighted by connection strength (positive) and myelin (negative) which were robust to controlling for edge length; (3) whole-brain inverse relationships with myelin for networks weighted by connection strength and neurite density independent of edge length; and (4) the absence of a rich club in R_1 and FA networks. All weighted SC networks showed a strong spatial dependence and small-world architecture. Collectively, these results support the overall conclusion that SC networks weighted by edge caliber (e.g., SIFT2 and COMMIT) and myelin (e.g., R_1) can be used to quantify non-overlapping subsets of white matter structural features related to FC supporting their joint utilization in modeling function.

365

366 ***COMMIT vs SIFT2: The Superior Estimate of Connectivity Strength?***

367 A principal goal of this work is to identify what, if any, advantage over NoS is provided by the
368 global optimization methods SIFT2 and COMMIT. NoS has previously been used to inform the
369 strength of interregional coupling in computational models of function (e.g., (Honey et al.,
370 2009)). However, important limitations restrict model interpretation. Besides suffering from a
371 range of biases related to the position, size, shape and length of white matter tracts (Girard et al.,
372 2014), NoS varies as a function of tracking parameters limiting its specificity for white matter
373 structural features (Jones, 2010; Jones et al., 2013). SIFT2 and COMMIT reportedly restore the
374 quantitative link between connectome edge weights and white matter structural features related
375 to connection strength. Our results show that when network density is uniform across structural
376 metrics, COMMIT shows greater subject-specificity, edge weight contrast, correlation with
377 myelin, small-worldness and rich club coefficient relative to SIFT2. This supports the hypothesis
378 that using COMMIT instead of NoS to modulate the strength of interregional coupling in
379 computational models of function will yield the greatest improvement in model fit.

380

381

382 ***Myelin Complements Connection Strength in Predicting FC***

383 Despite the differences between COMMIT, SIFT2 and NoS; our results indicate that their edge
384 weights show roughly equivalent positive correlations with FC over the whole brain. R_1 was
385 negatively correlated with FC. Significant evidence indicates a link between cerebral myelin and
386 FC including: a relationship between intracortical myelin and FC (Huntenburg et al., 2017;
387 Wang et al., 2019); the prediction of cognition (Sonya Bells et al., 2017; Caeyenberghs et al.,

2016) and FC-derived components (Messaritaki et al., 2021) with myelin-sensitive metrics; and a relationship between damaged myelin sheaths and greater conduction delays in multiple sclerosis (Sorrentino et al., 2022). At the cellular-level, myelin contributes to conduction velocity (Huxley & Stämpfli, 1949), metabolic support (Nave & Werner, 2014) and plasticity (Gibson et al., 2018), all of which could be argued to support brain function. Myelin plasticity in particular can be described in terms of "activity-dependence", whereby an increase in the functional activity of a given circuit stimulates cellular signaling cascades promoting greater myelination (Douglas Fields, 2015; Mount & Monje, 2017). Coupled with our results, this complex mix of functional roles supports the idea that structure-function models will be improved by integrating measures of myelin and connection strength.

Tract g-ratio and Edge Caliber are Inversely Related to Length

When controlling for edge length, we found an inverse relationship between R_1 and COMMIT over the whole brain in all subjects and at the group level. This suggests that the aggregate g-ratio of a white matter tract may increase with edge caliber. At the cellular-level, the diameter of an axon and the thickness of its myelin sheath show nearly a linear relationship over a broad range of smaller diameter axons which becomes increasingly nonlinear as axon diameter increases (Berthold et al., 1983; Hildebrand & Hahn, 1978). In general, increasing axon diameter tends to outpace increasing myelin thickness i.e., g-ratio tends to increase with increasing axon caliber (Hildebrand & Hahn, 1978). Our findings suggest that this cellular-level principle may extend to the systems level: increases in edge caliber tend to outpace changes in the myelin content resulting in a concomitant increase in the g-ratio of white matter tracts.

We localized the inverse relationship between R_1 and COMMIT to the shortest edges i.e., the g-ratio was the highest in the shortest connections. This result is supported by a previous imaging study showing the highest g-ratio in "local" connections (Mancini et al., 2018). In general, we found that R_1 increased and COMMIT decreased with increasing edge length. Both of these trends fit well with theories of brain wiring economy in which the energetic cost of maintaining biological material increases with connection length (Bullmore & Sporns, 2012). This natural pressure acts to reduce the total axonal volume of longer white matter bundles. Increasing the myelin content of longer tracts comes at a cost as well, but this may be at least partially offset as increasing myelin content reduces the total membrane surface area along which expensive electrochemical gradients must be maintained (Bullmore & Sporns, 2012). Although, a cost-benefit analysis of the energetics of myelination concluded that the energetic cost of myelin maintenance outweighs any savings on action potentials (Harris & Attwell, 2012). This suggests that higher myelination of longer edges may be better explained as a mechanism to provide trophic support (Nave & Werner, 2014) to vital inter-regional connections (Martijn P. Van Den Heuvel et al., 2012) or to reduce conduction delays.

Edge Weight Variance Decreases with Edge Length in Most Weighted Structural Networks?

White matter features related to myelin content, connection strength and neurite density tend to become more consistent across tracts as tract length increases. Greater variability in the weights of the shortest connections could result from a higher proportion of false positive streamlines influencing these edge weights. For SIFT2 and COMMIT, streamline weight computation

becomes increasingly unstable with decreasing length as fewer voxels contribute to the fit. However, this result could also be explained more generally by contrasting the roles of shorter and longer connections in the brain. Shorter white matter tracts connect brain regions near each other in space e.g., within the same module. Just as we might expect the characteristics of smaller roads and streets (e.g., width, building materials, markings, signs, sidewalks, etc.) to vary by neighborhood and city, we might also expect the morphology of shorter white matter connections to change as the functional specialization of any given region or module changes. On the other hand, longer tracts (i.e., the freeways of the brain) may overlap more in both their functional role and morphological features relative to shorter connections, hence lower edge weight variability. Breaking with the above pattern, FA and RD showed the highest edge weight variance in the longest connections. Given that structural measures derived using a voxel-wise diffusion tensor model are particularly sensitive to the white matter "architectural paradigm" (Jones et al., 2013), these results suggest that white matter features related to fiber orientation and geometry actually diverge with increasing tract length.

The Absence of a Rich Club in R_1 and FA

Group-level R_1 and FA did not show a normalized weighted rich club for any degree k. Higher myelination in the white matter tracts connecting rich club nodes has previously been reported (Collin et al., 2014); however, methodological differences limit comparability. A rich club has previously been reported in FA-weighted networks using similar methods to ours (Martijn P. van den Heuvel & Sporns, 2011). The source of this disagreement could potentially be attributed to differences in our tractography algorithm, parcellation or null network computation.

In weighted rich-club detection, the identification of a densely connected core is independent of edge weight (depends only on node degree), but the designation of this subnetwork as a rich club requires that it contains a higher-than-chance proportion of the strongest edges from the full network. Indeed, this is the case over a broad range of degree k for COMMIT. Over the same range of k, the normalized rich-club curves for R_1 and FA are inverted about the threshold value of 1 with respect to COMMIT. This implies that the subnetwork found at a given k in this range contains edges which tend to show higher COMMIT and lower R_1 edge weights than expected by chance. We previously showed edgewise inverse correlations between R_1 and COMMIT which were robust to controlling for edge length. We also showed that R_1 and FA are positively correlated under these same conditions. In this light, it is not surprising that the edges connecting rich-club nodes tend to show opposite trends in R_1- and FA-weighting with respect to COMMIT. Nonetheless, it is possible that the lack of a rich club in our myelin-weighted network is an artifact of tractometry. Future work will attempt to replicate this result using myelin-weighted networks computed with a different methodology (Schiavi et al., 2022).

Limitations

Streamline tractography is known to suffer from several important biases including both false positive and negative streamlines which can influence downstream analyses (Maier-Hein et al., 2017; Schilling et al., 2019; Sotiropoulos & Zalesky, 2019; Zalesky et al., 2016). Through probabilistic tracking, we opted to minimize false negatives while maximizing false positives. This allowed us to implement careful streamline- and edge-filtering strategies in post-processing to address this known bias. Still, without a ground truth, we cannot quantify the extent to which

480 we were successful in mitigating this issue, nor can we guarantee that we did not erroneously
481 filter true positive streamlines or edges. All processing and filtering methods were consistent and
482 network density was uniform across weighted structural networks. Thus, any major tractography
483 bias should be as homogeneous as possible across networks.
484
485 Tractometry-derived brain networks suffer from widespread partial volume effects. The net
486 effect of this bias is well understood and is apparent in our results and previous work (De Santis
487 et al., 2014; Schiavi et al., 2022). Nonetheless, this method was included here as our goal was to
488 characterize widely used structural connectivity methods. New techniques for reducing this bias
489 are currently being developed which allow for the estimation of tract-specific microstructural
490 features (e.g., (Barakovic, Girard, et al., 2021; Barakovic, Tax, et al., 2021; De Santis et al.,
491 2016; Leppert et al., 2021; Schiavi et al., 2022)).
492
493
494 ***Conclusion***
495 We presented a thorough characterization of weighted SC networks. Overall, our findings
496 support the joint use of SC networks weighted by connection strength and myelin in predicting
497 FC. In particular, using the COMMIT algorithm to quantify connection strength shows promise.
498 Beyond R_1, there are a wide array of myelin sensitive metrics that could be used to compute
499 useful myelin-weighted networks. The integration of this microstructure-weighted connectivity
500 approach into structure-function models will advance the mechanistic interpretation of both the
501 function and dysfunction of the living human brain.
502

MATERIALS and METHODS

These data are available for download (https://portal.conp.ca/dataset?id=projects/mica-mics). See Royer et al. (Royer et al., 2022), Cruces et al. (Cruces et al., 2022) for full details of data acquisition and processing. All data processing and analysis code is openly available at https://github.com/TardifLab/Weighted-SC-Networks.

Data Acquisition & Preprocessing

Multimodal MRI data was collected in 50 healthy volunteers at 3 Tesla as follows:

- T_1-weighted (T_1w) anatomical: 3D magnetization-prepared rapid gradient-echo sequence (MP-RAGE; 0.8mm isotropic)
- Multi-shell diffusion-weighted imaging (DWI): 2D pulsed gradient spin-echo echo-planar imaging sequence (1.6mm isotropic); three shells with b-values 300, 700, and 2000s/mm^2 and diffusion directions 10, 40, and 90
- 7 minutes of resting-state functional MRI: multi-band accelerated 2D-BOLD gradient echo echo-planar sequence (3mm isotropic)
- A quantitative T_1 map: 3D-MP2RAGE sequence (Marques et al., 2010) (0.8mm isotropic)

The multi-modal processing pipeline *micapipe* (Cruces et al., 2022) (https://micapipe.readthedocs.io/) was used to preprocess diffusion, anatomical, and functional images. Functional data derivatives were obtained in parcellated FC matrix form.

526

527

528 ***Tractography and Microstructural Metrics***

529 To estimate structural connectomes, anatomically constrained tractography (R. E. Smith et al.,
530 2012) was performed on the normalized white matter FOD image using the probabilistic
531 algorithm iFOD2 (J.-D. Tournier et al., 2010). Tractograms of 5 million streamlines were
532 generated by seeding the gray-white matter interface using the following parameters:
533 maxlength=400, minlength=10, angle=22.5, step=0.5, cutoff=0.06, backtrack, crop_at_gmwmi
534 (gray-matter-white-matter interface). These tractograms were filtered in a two-stage process. (1)
535 a whole-brain connectome weighted by NoS was computed then decomposed into its composite
536 streamlines to derive a new tractogram in which any streamline which failed to connect two gray
537 matter ROIs was excluded. This "streamline-filtering" step typically resulted in approximately a
538 5% decrease in the size of the tractogram (~250k streamlines removed) and was undertaken to
539 ensure that these erroneous streamlines did not affect the COMMIT model. Streamline-filtered
540 tractograms were used to compute NoS and were used as inputs to both the SIFT2 and COMMIT
541 models. SIFT2 determines the effective cross-sectional area of each streamline such that the
542 streamline density throughout the white matter fits the fiber densities estimated using spherical
543 deconvolution. COMMIT was run using a Stick-Zeppelin-Ball forward model and default
544 settings (see https://github.com/daducci/COMMIT). Using the simplifying assumption that
545 structural features are constant along the length of a streamline, COMMIT can be used to
546 compute a weight for each streamline representing their respective proportion of the global
547 diffusion signal i.e., the cross-sectional area of their intracellular compartment. (2) Any
548 streamline with a COMMIT weight $< 1e^{-12}$ (machine precision 0) was interpreted as a false

positive and filtered from the tractogram. This streamline-level COMMIT-filtering step typically resulted in greater than a 90% decrease in the size of the tractogram with most containing between ~300-600k streamlines. COMMIT-filtered tractograms were used not only in the computation of COMMIT, but all tractometry networks as well. This additional filtering step was performed on COMMIT streamline weights only (not SIFT2) to reduce the impact of false positive streamlines in tractometry networks as much as possible.

Construction of Weighted Structural Networks

The streamline-specific SC networks were computed in the following manner: (1) NoS as the summed streamline count; (2) LoS as the mean streamline length; (3) SIFT2 as the sum of SIFT2 streamline weights; and (4) COMMIT as the length-weighted sum of COMMIT streamline weights as in (Schiavi et al., 2020). Explicitly, edgewise entries in COMMIT-weighted networks were computed as:

$$\alpha_{ij} = \frac{\sum_{k=1}^{N_{ij}} (x_{ij}^{k} * l_k)}{\bar{L}_{ij}},$$

where α_{ij} is the edge weight between nodes *i* and *j*; $\bar{L}_{ij}$ is the mean streamline length; N_{ij} is the number of streamlines; x_{ij}^{k} is the COMMIT weight of streamline k; and l_k is its length. Edge weights in NoS, SIFT2 and COMMIT were normalized by node volume.

SC networks weighted by FA, RD, ICVF (Zhang et al., 2012) and R_1 were derived using multi-modal tractometry (S Bells et al., 2011). Streamline weights were computed by: (1) co-registering the tractogram and desired image; and (2) sampling the voxel-level aggregate value

along the length of each streamline. Edge weights were computed as the median along each streamline and the mean across streamlines by node pair. Voxel-wise measures of FA and RD were computed with a diffusion tensor model (Basser et al., 1994) and ICVF by applying the NODDI multi-compartment model (Zhang et al., 2012) to preprocessed DWI data (Daducci, Canales-Rodríguez, et al., 2015).

The 400-node Schaefer (Schaefer et al., 2018) cortical parcellation is used in all results. Subcortical ROIs corresponded to 7 bilateral regions (14 nodes) including the amygdala, thalamus, caudate, accumbens, putamen, hippocampus, and pallidum. A single static, zero-lag FC network was derived by product-moment pairwise Pearson cross-correlation of node-averaged time series. FC network edge weights were Fisher Z-transformed.

Connectome post-processing

All SC networks were thresholded at the edge level within subject by: (1) setting edges = 0 in all weighted SC networks if they had a COMMIT edge weight < $1e^{-12}$; and (2) applying a 50% uniform threshold mask to facilitate group-consensus averaging. This minimized differences in binary structural network density across subjects and enforced uniform density across weighted SC networks at the group level and within subject. COMMIT was used for this filter as it had the lowest connection density to start.

Network Analysis

Network analysis was performed using tools (Rubinov & Sporns, 2010) based on graph theory (Fornito et al., 2013; Sporns, 2018). Measures of clustering coefficient and path length were normalized against 50 degree and strength preserving null networks. Clustering coefficient was normalized within node then averaged across nodes to obtain a scalar value per network. The following weight (W_{ij}) to length (L_{ij}) transform was used in path length computation: $L_{ij} = -\log(W_{ij})$. Weighted rich club curves were normalized against 1000 degree and strength preserving null networks. The edges in all degree and strength preserving null networks were rewired $1e^6$ times total, and the strength sequence was approximated using simulated annealing. Rich club curves were normalized in binary networks against 1000 degree preserving null networks in which each edge was rewired 100 times. All edge rewiring followed the Maslov & Sneppen rewiring model (Maslov & Sneppen, 2002). Similar to (M. P. van den Heuvel et al., 2010), hubness scores (0-5) were computed as 1 point for all nodes showing top 20% strength, betweenness, closeness or eigenvector centrality; and lowest 20% clustering coefficient.

ACKNOWLEDGMENTS

We acknowledge research support from the National Science and Engineering Research Council of Canada (NSERC Discovery-1304413, DGECR-2018-00216), the CIHR (FDN-154298, PJT-174995), SickKids Foundation (NI17-039), Azrieli Center for Autism Research (ACAR-TACC), Brain Canada, Fonds de recherche du Québec – Santé (FRQ-S), Healthy Brains for Healthy Lives, and the Tier-2 Canada Research Chairs program.

REFERENCES

Alexander, D. C., Dyrby, T. B., Nilsson, M., & Zhang, H. (2019). Imaging brain microstructure with diffusion MRI: practicality and applications. *NMR in Biomedicine*, *32*(4), 1–26. https://doi.org/10.1002/nbm.3841

Alexander, D. C., Hubbard, P. L., Hall, M. G., Moore, E. A., Ptito, M., Parker, G. J. M., & Dyrby, T. B. (2010). Orientationally invariant indices of axon diameter and density from diffusion MRI. *NeuroImage*, *52*(4), 1374–1389. https://doi.org/10.1016/j.neuroimage.2010.05.043

Assaf, Y., Blumenfeld-Katzir, T., Yovel, Y., & Basser, P. J. (2008). AxCaliber: A method for measuring axon diameter distribution from diffusion MRI. *Magnetic Resonance in Medicine*, *59*(6), 1347–1354. https://doi.org/10.1002/mrm.21577

Barakovic, M., Girard, G., Schiavi, S., Romascano, D., Descoteaux, M., Granziera, C., Jones, D. K., Innocenti, G. M., Thiran, J.-P., & Daducci, A. (2021). Bundle-Specific Axon Diameter Index as a New Contrast to Differentiate White Matter Tracts. *Frontiers in Neuroscience*, *15*(June), 1–13. https://doi.org/10.3389/fnins.2021.646034

Barakovic, M., Tax, C. M. W., Rudrapatna, U., Chamberland, M., Rafael-Patino, J., Granziera, C., Thiran, J. P., Daducci, A., Canales-Rodríguez, E. J., & Jones, D. K. (2021). Resolving bundle-specific intra-axonal T2 values within a voxel using diffusion-relaxation tract-based estimation. *NeuroImage*, *227*(September 2020), 117617. https://doi.org/10.1016/j.neuroimage.2020.117617

Basser, P. J. (1995). Inferring microstructural features and the physiological state of tissues from diffusion-weighted images. *NMR in Biomedicine*, *8*(7), 333–344. https://doi.org/10.1002/nbm.1940080707

Basser, P. J., Mattiello, J., & Lebihan, D. (1994). Estimation of the Effective Self-Diffusion Tensor from the NMR Spin Echo. In *Journal of Magnetic Resonance, Series B* (Vol. 103, Issue 3, pp. 247–254). https://doi.org/10.1006/jmrb.1994.1037

Bassett, D. S., & Bullmore, E. (2006). Small-world brain networks. *Neuroscientist*, *12*(6), 512–523. https://doi.org/10.1177/1073858406293182

Bassett, D. S., & Bullmore, E. T. (2017). Small-World Brain Networks Revisited. *Neuroscientist*, *23*(5), 499–516. https://doi.org/10.1177/1073858416667720

Bells, S, Cercignani, M., Deoni, S., & Assaf, Y. (2011). "Tractometry" – comprehensive multi-modal quantitative assessment of white matter along specific tracts. *Proceedings of the International Society for Magnetic Resonance in Medicine*, *19*(2009), 678. http://cds.ismrm.org/protected/11MProceedings/files/678.pdf

Bells, Sonya, Lefebvre, J., Prescott, S. A., Dockstader, C., Bouffet, E., Skocic, J., Laughlin, S., & Mabbott, D. J. (2017). Changes in white matter microstructure impact cognition by disrupting the ability of neural assemblies to synchronize. *Journal of Neuroscience*, *37*(34), 8227–8238. https://doi.org/10.1523/jneurosci.0560-17.2017

Berthold, C. H., Nilsson, I., & Rydmark, M. (1983). Axon diameter and myelin sheath thickness in nerve fibres of the ventral spinal root of the seventh lumbar nerve of the adult and developing cat. *Journal of Anatomy*, *136*(Pt 3), 483–508. https://pubmed.ncbi.nlm.nih.gov/6885614/

Biswal, B., Zerrin Yetkin, F., Haughton, V. M., & Hyde, J. S. (1995). Functional connectivity in the motor cortex of resting human brain using echo-planar mri. *Magnetic Resonance in Medicine*, *34*(4), 537–541. https://doi.org/10.1002/mrm.1910340409

Boshkovski, T., Kocarev, L., Cohen-Adad, J., Mišić, B., Lehéricy, S., Stikov, N., & Mancini, M. (2021). The R1-weighted connectome: complementing brain networks with a myelin-sensitive measure. *Network Neuroscience*, *5*(2), 358–372. https://doi.org/10.1162/netn_a_00179

Bullmore, E., & Sporns, O. (2012). The economy of brain network organization. *Nature Reviews Neuroscience*, *13*(5), 336–349. https://doi.org/10.1038/nrn3214

Cabral, J., Kringelbach, M. L., & Deco, G. (2017). Functional connectivity dynamically evolves on multiple time-scales over a static structural connectome: Models and mechanisms. *NeuroImage*, *160*(March), 84–96. https://doi.org/10.1016/j.neuroimage.2017.03.045

654 Caeyenberghs, K., Metzler-Baddeley, C., Foley, S., & Jones, D. K. (2016). Dynamics of the human structural connectome underlying working
655 memory training. *Journal of Neuroscience*, *36*(14), 4056–4066. https://doi.org/10.1523/JNEUROSCI.1973-15.2016
656 Collin, G., Sporns, O., Mandl, R. C. W., & Van Den Heuvel, M. P. (2014). Structural and functional aspects relating to cost and benefit of rich
657 club organization in the human cerebral cortex. *Cerebral Cortex*, *24*(9), 2258–2267. https://doi.org/10.1093/cercor/bht064
658 Cruces, R. R., Royer, J., Herholz, P., Larivière, S., Vos de Wael, R., Paquola, C., Benkarim, O., Park, B., Degré-Pelletier, J., Nelson, M. C.,
659 DeKraker, J., Leppert, I. R., Tardif, C., Poline, J.-B., Concha, L., & Bernhardt, B. C. (2022). Micapipe: A pipeline for multimodal
660 neuroimaging and connectome analysis. *NeuroImage*, *263*(August), 119612. https://doi.org/10.1016/j.neuroimage.2022.119612
661 Daducci, A., Canales-Rodríguez, E. J., Zhang, H., Dyrby, T. B., Alexander, D. C., & Thiran, J. P. (2015). Accelerated Microstructure Imaging via
662 Convex Optimization (AMICO) from diffusion MRI data. *NeuroImage*, *105*, 32–44. https://doi.org/10.1016/j.neuroimage.2014.10.026
663 Daducci, A., Dal Palu, A., Lemkaddem, A., & Thiran, J. P. (2013). A convex optimization framework for global tractography. *Proceedings -*
664 *International Symposium on Biomedical Imaging*, 524–527. https://doi.org/10.1109/ISBI.2013.6556527
665 Daducci, A., Dal Palù, A., Lemkaddem, A., & Thiran, J. P. (2015). COMMIT: Convex optimization modeling for microstructure informed
666 tractography. *IEEE Transactions on Medical Imaging*, *34*(1), 246–257. https://doi.org/10.1109/TMI.2014.2352414
667 de Reus, M. A., & van den Heuvel, M. P. (2014). Simulated rich club lesioning in brain networks: A scaffold for communication and integration?
668 *Frontiers in Human Neuroscience*, *8*(AUG), 1–5. https://doi.org/10.3389/fnhum.2014.00647
669 De Santis, S., Assaf, Y., Jeurissen, B., Jones, D. K., & Roebroeck, A. (2016). T1 relaxometry of crossing fibres in the human brain. *NeuroImage*,
670 *141*, 133–142. https://doi.org/10.1016/j.neuroimage.2016.07.037
671 De Santis, S., Drakesmith, M., Bells, S., Assaf, Y., & Jones, D. K. (2014). Why diffusion tensor MRI does well only some of the time: Variance
672 and covariance of white matter tissue microstructure attributes in the living human brain. *NeuroImage*, *89*, 35–44.
673 https://doi.org/10.1016/j.neuroimage.2013.12.003
674 Deligianni, F., Carmichael, D. W., Zhang, G. H., Clark, C. A., & Clayden, J. D. (2016). NODDI and tensor-based microstructural indices as
675 predictors of functional connectivity. *PLoS ONE*, *11*(4), 1–17. https://doi.org/10.1371/journal.pone.0153404
676 Douglas Fields, R. (2015). A new mechanism of nervous system plasticity: activity-dependent myelination. *Nature Reviews Neuroscience*,
677 *16*(12), 756–767. https://doi.org/10.1007/s11065-015-9294-9.Functional
678 Drakesmith, M., Harms, R., Rudrapatna, S. U., Parker, G. D., Evans, C. J., & Jones, D. K. (2019). Estimating axon conduction velocity in vivo
679 from microstructural MRI. *NeuroImage*, *203*(March), 116186. https://doi.org/10.1016/j.neuroimage.2019.116186
680 Finn, E. S., Huber, L., Jangraw, D. C., Molfese, P. J., & Bandettini, P. A. (2019). Layer-dependent activity in human prefrontal cortex during
681 working memory. *Nature Neuroscience*, *22*(10), 1687–1695. https://doi.org/10.1038/s41593-019-0487-z
682 Fornito, A., Zalesky, A., & Breakspear, M. (2013). Graph analysis of the human connectome: Promise, progress, and pitfalls. *NeuroImage*, *80*,
683 426–444. https://doi.org/10.1016/j.neuroimage.2013.04.087
684 Fornito, A., Zalesky, A., & Breakspear, M. (2015). The connectomics of brain disorders. *Nature Reviews Neuroscience*, *16*(3), 159–172.
685 https://doi.org/10.1038/nrn3901
686 Fornito, A., Zalesky, A., & Bullmore, E. T. (2016). Fundamentals of Brain Network Analysis. In *Fundamentals of Brain Network Analysis*.
687 Elsevier. https://doi.org/10.1016/C2012-0-06036-X
688 Frigo, M., Deslauriers-Gauthier, S., Parker, D., Ismail, A. A. O., Kim, J. J., Verma, R., & Deriche, R. (2020). Diffusion MRI tractography

filtering techniques change the topology of structural connectomes. *Journal of Neural Engineering*, *17*(6). https://doi.org/10.1088/1741-2552/abc29b

Friston, K. J. (2011). Functional and effective connectivity: a review. *Brain Connectivity*, *1*(1), 13–36. https://doi.org/10.1089/brain.2011.0008

Gibson, E. M., Geraghty, A. C., & Monje, M. (2018). Bad wrap: Myelin and myelin plasticity in health and disease. In *Developmental Neurobiology* (Vol. 78, Issue 2, pp. 123–135). John Wiley and Sons Inc. https://doi.org/10.1002/dneu.22541

Girard, G., Whittingstall, K., Deriche, R., & Descoteaux, M. (2014). Towards quantitative connectivity analysis: Reducing tractography biases. *NeuroImage*, *98*, 266–278. https://doi.org/10.1016/j.neuroimage.2014.04.074

Gordon, E. M., Laumann, T. O., Gilmore, A. W., Newbold, D. J., Greene, D. J., Berg, J. J., Ortega, M., Hoyt-Drazen, C., Gratton, C., Sun, H., Hampton, J. M., Coalson, R. S., Nguyen, A. L., McDermott, K. B., Shimony, J. S., Snyder, A. Z., Schlaggar, B. L., Petersen, S. E., Nelson, S. M., & Dosenbach, N. U. F. (2017). Precision Functional Mapping of Individual Human Brains. *Neuron*, *95*(4), 791-807.e7. https://doi.org/10.1016/j.neuron.2017.07.011

Greicius, M. D., Krasnow, B., Reiss, A. L., & Menon, V. (2003). Functional connectivity in the resting brain: A network analysis of the default mode hypothesis. *Proceedings of the National Academy of Sciences of the United States of America*, *100*(1), 253–258. https://doi.org/10.1073/pnas.0135058100

Griffa, A., & Van den Heuvel, M. P. (2018). Rich-club neurocircuitry: function, evolution, and vulnerability. *Dialogues in Clinical Neuroscience*, *20*(2), 121–132. https://doi.org/10.31887/DCNS.2018.20.2/agriffa

Hampson, M., Driesen, N. R., Skudlarski, P., Gore, J. C., & Constable, R. T. (2006). Brain connectivity related to working memory performance. *Journal of Neuroscience*, *26*(51), 13338–13343. https://doi.org/10.1523/JNEUROSCI.3408-06.2006

Harris, J. J., & Attwell, D. (2012). The energetics of CNS white matter. *Journal of Neuroscience*, *32*(1), 356–371. https://doi.org/10.1523/JNEUROSCI.3430-11.2012

Heath, F., Hurley, S. A., Johansen-Berg, H., & Sampaio-Baptista, C. (2018). Advances in noninvasive myelin imaging. *Developmental Neurobiology*, *78*(2), 136–151. https://doi.org/10.1002/dneu.22552

Hildebrand, C., & Hahn, R. (1978). Relation between myelin sheath thickness and axon size in spinal cord white matter of some vertebrate species. *Journal of the Neurological Sciences*, *38*(3), 421–434. https://doi.org/10.1016/0022-510X(78)90147-8

Hodgkin, A. L., & Huxley, A. F. (1952). A quantitative description of membrane current and its application to conduction and excitation in nerve. *The Journal of Physiology*, *117*(4), 500–544. https://doi.org/10.1113/jphysiol.1952.sp004764

Honey, C. J., Sporns, O., Cammoun, L., Gigandet, X., Thiran, J. P., Meuli, R., & Hagmann, P. (2009). Predicting human resting-state functional connectivity from structural connectivity. *Proceedings of the National Academy of Sciences of the United States of America*, *106*(6), 2035–2040. https://doi.org/10.1073/pnas.0811168106

Huntenburg, J. M., Bazin, P. L., Goulas, A., Tardif, C. L., Villringer, A., & Margulies, D. S. (2017). A Systematic Relationship Between Functional Connectivity and Intracortical Myelin in the Human Cerebral Cortex. *Cerebral Cortex*, *27*(2), 981–997. https://doi.org/10.1093/cercor/bhx030

Huxley, A. F., & Stämpfli, R. (1949). Evidence for saltatory conduction in peripheral myelinated nerve fibres. *The Journal of Physiology*, *108*(3), 315–339. http://www.ncbi.nlm.nih.gov/pubmed/16991863

Jeurissen, B., Descoteaux, M., Mori, S., & Leemans, A. (2017). Diffusion MRI fiber tractography of the brain. *NMR in Biomedicine*, *32*(4), 1–22.

https://doi.org/10.1002/nbm.3785

Jeurissen, B., Leemans, A., Tournier, J. D., Jones, D. K., & Sijbers, J. (2012). Investigating the prevalence of complex fiber configurations in white matter tissue with diffusion magnetic resonance imaging. *Human Brain Mapping*, *34*(11), 2747–2766. https://doi.org/10.1002/hbm.22099

Jones, D. K. (2010). Challenges and limitations of quantifying brain connectivity in vivo with diffusion MRI. *Imaging in Medicine*, *2*(3), 341–355. https://doi.org/10.2217/iim.10.21

Jones, D. K., Knösche, T. R., & Turner, R. (2013). White matter integrity, fiber count, and other fallacies: The do's and don'ts of diffusion MRI. *NeuroImage*, *73*, 239–254. https://doi.org/10.1016/j.neuroimage.2012.06.081

Kim, D. J., & Min, B. K. (2020). Rich-club in the brain's macrostructure: Insights from graph theoretical analysis. *Computational and Structural Biotechnology Journal*, *18*, 1761–1773. https://doi.org/10.1016/j.csbj.2020.06.039

Larivière, S., Paquola, C., Park, B. yong, Royer, J., Wang, Y., Benkarim, O., Vos de Wael, R., Valk, S. L., Thomopoulos, S. I., Kirschner, M., Lewis, L. B., Evans, A. C., Sisodiya, S. M., McDonald, C. R., Thompson, P. M., & Bernhardt, B. C. (2021). The ENIGMA Toolbox: multiscale neural contextualization of multisite neuroimaging datasets. *Nature Methods*, *18*(7), 698–700. https://doi.org/10.1038/s41592-021-01186-4

Leppert, I. R., Andrews, D. A., Campbell, J. S. W., Park, D. J., Pike, G. B., Polimeni, J. R., & Tardif, C. L. (2021). Efficient whole-brain tract-specific T1 mapping at 3T with slice-shuffled inversion-recovery diffusion-weighted imaging. *Magnetic Resonance in Medicine*, *86*(2), 738–753. https://doi.org/10.1002/mrm.28734

Liégeois, R., Li, J., Kong, R., Orban, C., Van De Ville, D., Ge, T., Sabuncu, M. R., & Yeo, B. T. T. (2019). Resting brain dynamics at different timescales capture distinct aspects of human behavior. *Nature Communications*, *10*(1). https://doi.org/10.1038/s41467-019-10317-7

Liu, Z. Q., Vázquez-Rodríguez, B., Spreng, R. N., Bernhardt, B. C., Betzel, R. F., & Misic, B. (2022). Time-resolved structure-function coupling in brain networks. *Communications Biology*, *5*(1), 1–10. https://doi.org/10.1038/s42003-022-03466-x

Maier-Hein, K. H., Neher, P. F., Houde, J. C., Côté, M. A., Garyfallidis, E., Zhong, J., Chamberland, M., Yeh, F. C., Lin, Y. C., Ji, Q., Reddick, W. E., Glass, J. O., Chen, D. Q., Feng, Y., Gao, C., Wu, Y., Ma, J., Renjie, H., Li, Q., … Descoteaux, M. (2017). The challenge of mapping the human connectome based on diffusion tractography. *Nature Communications*, *8*(1). https://doi.org/10.1038/s41467-017-01285-x

Mancini, M., Giulietti, G., Dowell, N., Spanò, B., Harrison, N., Bozzali, M., & Cercignani, M. (2018). Introducing axonal myelination in connectomics: A preliminary analysis of g-ratio distribution in healthy subjects. *NeuroImage*, *182*, 351–359. https://doi.org/10.1016/j.neuroimage.2017.09.018

Mancini, M., Karakuzu, A., Cohen-Adad, J., Cercignani, M., Nichols, T. E., & Stikov, N. (2020). An interactive meta-analysis of MRI biomarkers of myelin. *ELife*, *9*, 1–23. https://doi.org/10.7554/eLife.61523

Margulies, D. S., Ghosh, S. S., Goulas, A., Falkiewicz, M., Huntenburg, J. M., Langs, G., Bezgin, G., Eickhoff, S. B., Castellanos, F. X., Petrides, M., Jefferies, E., & Smallwood, J. (2016). Situating the default-mode network along a principal gradient of macroscale cortical organization. *Proceedings of the National Academy of Sciences of the United States of America*, *113*(44), 12574–12579. https://doi.org/10.1073/pnas.1608282113

Marques, J. P., Kober, T., Krueger, G., van der Zwaag, W., Van de Moortele, P. F., & Gruetter, R. (2010). MP2RAGE, a self bias-field corrected

sequence for improved segmentation and T1-mapping at high field. *NeuroImage*, *49*(2), 1271–1281. https://doi.org/10.1016/j.neuroimage.2009.10.002

Maslov, S., & Sneppen, K. (2002). Specificity and stability in topology of protein networks. *Science*, *296*(5569), 910–913. https://doi.org/10.1126/science.1065103

Messaritaki, E., Foley, S., Schiavi, S., Magazzini, L., Routley, B., Jones, D. K., & Singh, K. D. (2021). Predicting meg resting-state functional connectivity from microstructural information. *Network Neuroscience*, *5*(2), 477–504. https://doi.org/10.1162/netn_a_00187

Moore, S., Meschkat, M., Ruhwedel, T., Trevisiol, A., Tzvetanova, I. D., Battefeld, A., Kusch, K., Kole, M. H. P., Strenzke, N., Möbius, W., de Hoz, L., & Nave, K. A. (2020). A role of oligodendrocytes in information processing. *Nature Communications*, *11*(1), 1–15. https://doi.org/10.1038/s41467-020-19152-7

Mottershead, J. P., Schmierer, K., Clemence, M., Thornton, J. S., Scaravilli, F., Barker, G. J., Tofts, P. S., Newcombe, J., Cuzner, M. L., Ordidge, R. J., McDonald, W. I., & Miller, D. H. (2003). High field MRI correlates of myelin content and axonal density in multiple sclerosis: A post-mortem study of the spinal cord. *Journal of Neurology*, *250*(11), 1293–1301. https://doi.org/10.1007/s00415-003-0192-3

Mount, C. W., & Monje, M. (2017). Wrapped to Adapt: Experience-Dependent Myelination. *Neuron*, *95*(4), 743–756. https://doi.org/10.1016/j.neuron.2017.07.009

Nave, K. A., & Werner, H. B. (2014). Myelination of the nervous system: Mechanisms and functions. *Annual Review of Cell and Developmental Biology*, *30*, 503–533. https://doi.org/10.1146/annurev-cellbio-100913-013101

Pumphrey, R. J., & Young, J. Z. (1938). The Rates Of Conduction Of Nerve Fibres Of Various Diameters In Cephalopods. *Journal of Experimental Biology*, *15*(4), 453–466. https://doi.org/10.1242/jeb.15.4.453

Royer, J., Rodríguez-Cruces, R., Tavakol, S., Larivière, S., Herholz, P., Li, Q., Vos de Wael, R., Paquola, C., Benkarim, O., Park, B., Lowe, A. J., Margulies, D., Smallwood, J., Bernasconi, A., Bernasconi, N., Frauscher, B., & Bernhardt, B. C. (2022). An Open MRI Dataset For Multiscale Neuroscience. *Scientific Data*, *9*(1), 569. https://doi.org/10.1038/s41597-022-01682-y

Rubinov, M., & Sporns, O. (2010). Complex network measures of brain connectivity: Uses and interpretations. *NeuroImage*, *52*(3), 1059–1069. https://doi.org/10.1016/j.neuroimage.2009.10.003

Schaefer, A., Kong, R., Gordon, E. M., Laumann, T. O., Zuo, X.-N., Holmes, A. J., Eickhoff, S. B., & Yeo, B. T. T. (2018). Local-Global Parcellation of the Human Cerebral Cortex from Intrinsic Functional Connectivity MRI. *Cerebral Cortex*, *28*(9), 3095–3114. https://doi.org/10.1093/cercor/bhx179

Schiavi, S., Lu, P., Weigel, M., Lutti, A., Jones, D. K., Kappos, L., Granziera, C., & Daducci, A. (2022). Bundle Myelin Fraction (BMF) Mapping of Different White Matter Connections Using Microstructure Informed Tractography. *NeuroImage*, 118922. https://doi.org/10.1016/j.neuroimage.2022.118922

Schiavi, S., Petracca, M., Battocchio, M., El Mendili, M. M., Paduri, S., Fleysher, L., Inglese, M., & Daducci, A. (2020). Sensory-motor network topology in multiple sclerosis: Structural connectivity analysis accounting for intrinsic density discrepancy. *Human Brain Mapping*, *41*(11), 2951–2963. https://doi.org/10.1002/hbm.24989

Schilling, K. G., Daducci, A., Maier-Hein, K., Poupon, C., Houde, J. C., Nath, V., Anderson, A. W., Landman, B. A., & Descoteaux, M. (2019). Challenges in diffusion MRI tractography – Lessons learned from international benchmark competitions. *Magnetic Resonance Imaging*, *57*(November 2018), 194–209. https://doi.org/10.1016/j.mri.2018.11.014

Smith, R. E., Tournier, J. D., Calamante, F., & Connelly, A. (2012). Anatomically-constrained tractography: Improved diffusion MRI streamlines tractography through effective use of anatomical information. *NeuroImage*, *62*(3), 1924–1938. https://doi.org/10.1016/j.neuroimage.2012.06.005

Smith, R. E., Tournier, J. D., Calamante, F., & Connelly, A. (2015). SIFT2: Enabling dense quantitative assessment of brain white matter connectivity using streamlines tractography. *NeuroImage*, *119*, 338–351. https://doi.org/10.1016/j.neuroimage.2015.06.092

Smith, S. M., Fox, P. T., Miller, K. L., Glahn, D. C., Fox, P. M., Mackay, C. E., Filippini, N., Watkins, K. E., Toro, R., Laird, A. R., & Beckmann, C. F. (2009). Correspondence of the brain's functional architecture during activation and rest. *Proceedings of the National Academy of Sciences of the United States of America*, *106*(31), 13040–13045. https://doi.org/10.1073/pnas.0905267106

Sorrentino, P., Petkoski, S., Sparaco, M., Troisi Lopez, E., Signoriello, E., Baselice, F., Bonavita, S., Pirozzi, M. A., Quarantelli, M., Sorrentino, G., & Jirsa, V. (2022). Whole-Brain Propagation Delays in Multiple Sclerosis, a Combined Tractography-Magnetoencephalography Study. *The Journal of Neuroscience : The Official Journal of the Society for Neuroscience*, *42*(47), 8807–8816. https://doi.org/10.1523/JNEUROSCI.0938-22.2022

Sotiropoulos, S. N., & Zalesky, A. (2019). Building connectomes using diffusion MRI: why, how and but. In *NMR in Biomedicine* (Vol. 32, Issue 4). https://doi.org/10.1002/nbm.3752

Sporns, O. (2010). Networks of the Brain. In *Networks of the Brain*. The MIT Press. https://doi.org/10.7551/mitpress/8476.001.0001

Sporns, O. (2011). The human connectome: A complex network. *Annals of the New York Academy of Sciences*, *1224*(1), 109–125. https://doi.org/10.1111/j.1749-6632.2010.05888.x

Sporns, O. (2018). Graph theory methods: applications in brain networks. *Dialogues in Clinical Neuroscience*, *20*(2), 111–120. https://doi.org/10.31887/DCNS.2018.20.2/osporns

Stikov, N., Campbell, J. S. W., Stroh, T., Lavelée, M., Frey, S., Novek, J., Nuara, S., Ho, M. K., Bedell, B. J., Dougherty, R. F., Leppert, I. R., Boudreau, M., Narayanan, S., Duval, T., Cohen-Adad, J., Picard, P. A., Gasecka, A., Côté, D., & Pike, G. B. (2015). In vivo histology of the myelin g-ratio with magnetic resonance imaging. *NeuroImage*, *118*, 397–405. https://doi.org/10.1016/j.neuroimage.2015.05.023

Stikov, N., Perry, L. M., Mezer, A., Rykhlevskaia, E., Wandell, B. A., Pauly, J. M., & Dougherty, R. F. (2011). Bound pool fractions complement diffusion measures to describe white matter micro and macrostructure. *NeuroImage*, *54*(2), 1112–1121. https://doi.org/10.1016/j.neuroimage.2010.08.068

Suárez, L. E., Markello, R. D., Betzel, R. F., & Misic, B. (2020). Linking Structure and Function in Macroscale Brain Networks. *Trends in Cognitive Sciences*. https://doi.org/10.1016/j.tics.2020.01.008

Thomas Yeo, B. T., Krienen, F. M., Sepulcre, J., Sabuncu, M. R., Lashkari, D., Hollinshead, M., Roffman, J. L., Smoller, J. W., Zöllei, L., Polimeni, J. R., Fisch, B., Liu, H., & Buckner, R. L. (2011). The organization of the human cerebral cortex estimated by intrinsic functional connectivity. *Journal of Neurophysiology*, *106*(3), 1125–1165. https://doi.org/10.1152/jn.00338.2011

Tournier, J.-D., Calamante, F., & Connelly, A. (2010). Improved probabilistic streamlines tractography by 2 nd order integration over fibre orientation distributions. *Ismrm*, *88*(2003), 2010. https://cds.ismrm.org/protected/10MProceedings/PDFfiles/1670_4298.pdf

Tournier, J. D., Mori, S., & Leemans, A. (2011). Diffusion tensor imaging and beyond. *Magnetic Resonance in Medicine*, *65*(6), 1532–1556. https://doi.org/10.1002/mrm.22924

van den Heuvel, M. P., Mandl, R. C. W., Stam, C. J., Kahn, R. S., & Hulshoff Pol, H. E. (2010). Aberrant Frontal and Temporal Complex

Network Structure in Schizophrenia: A Graph Theoretical Analysis. *Journal of Neuroscience*, *30*(47), 15915–15926. https://doi.org/10.1523/JNEUROSCI.2874-10.2010

Van Den Heuvel, Martijn P., Kahn, R. S., Goñi, J., & Sporns, O. (2012). High-cost, high-capacity backbone for global brain communication. *Proceedings of the National Academy of Sciences of the United States of America*, *109*(28), 11372–11377. https://doi.org/10.1073/pnas.1203593109

van den Heuvel, Martijn P., & Sporns, O. (2011). Rich-club organization of the human connectome. *Journal of Neuroscience*, *31*(44), 15775–15786. https://doi.org/https://doi.org/10.1523/JNEUROSCI.3539-11.2011

van den Heuvel, Martijn P., & Sporns, O. (2013). An anatomical substrate for integration among functional networks in human cortex. *Journal of Neuroscience*, *33*(36), 14489–14500. https://doi.org/10.1523/JNEUROSCI.2128-13.2013

Van Den Heuvel, Martijn P., Stam, C. J., Kahn, R. S., & Hulshoff Pol, H. E. (2009). Efficiency of functional brain networks and intellectual performance. *Journal of Neuroscience*, *29*(23), 7619–7624. https://doi.org/10.1523/JNEUROSCI.1443-09.2009

Vos de Wael, R., Benkarim, O., Paquola, C., Lariviere, S., Royer, J., Tavakol, S., Xu, T., Hong, S. J., Langs, G., Valk, S., Misic, B., Milham, M., Margulies, D. S., Smallwood, J., & Bernhardt, B. C. (2020). BrainSpace: a toolbox for the analysis of macroscale gradients in neuroimaging and connectomics datasets. *Communications Biology*, *3*(1). https://doi.org/10.1038/s42003-020-0794-7

Wang, P., Kong, R., Kong, X., Liégeois, R., Orban, C., Deco, G., van den Heuvel, M. P., & Thomas Yeo, B. T. (2019). Inversion of a large-scale circuit model reveals a cortical hierarchy in the dynamic resting human brain. *Science Advances*, *5*(1). https://doi.org/10.1126/sciadv.aat7854

Xia, M., Wang, J., & He, Y. (2013). BrainNet Viewer: A Network Visualization Tool for Human Brain Connectomics. *PLoS ONE*, *8*(7). https://doi.org/10.1371/journal.pone.0068910

Yeh, C. H., Smith, R. E., Liang, X., Calamante, F., & Connelly, A. (2016). Correction for diffusion MRI fibre tracking biases: The consequences for structural connectomic metrics. *NeuroImage*, *142*, 150–162. https://doi.org/10.1016/j.neuroimage.2016.05.047

Yeh, F. C., Badre, D., & Verstynen, T. (2016). Connectometry: A statistical approach harnessing the analytical potential of the local connectome. *NeuroImage*, *125*, 162–171. https://doi.org/10.1016/j.neuroimage.2015.10.053

Zalesky, A., Fornito, A., Cocchi, L., Gollo, L. L., van den Heuvel, M. P., & Breakspear, M. (2016). Connectome sensitivity or specificity: which is more important? *NeuroImage*, *142*, 407–420. https://doi.org/10.1016/j.neuroimage.2016.06.035

Zhang, H., Schneider, T., Wheeler-Kingshott, C. A., & Alexander, D. C. (2012). NODDI: Practical in vivo neurite orientation dispersion and density imaging of the human brain. *NeuroImage*, *61*(4), 1000–1016. https://doi.org/10.1016/j.neuroimage.2012.03.072